Reaction Pathway of the Trans-Acting Hepatitis Delta Virus Ribozyme: A Conformational Change Accompanies Catalysis†

Miguel J. B. Pereira, Dinari A. Harris, David Rueda, and Nils G. Walter*

Department of Chemistry, The University of Michigan, 930 North University Avenue, Ann Arbor, Michigan 48109-1055

Received October 23, 2001; Revised Manuscript Received November 20, 2001

ABSTRACT: The hepatitis delta virus (HDV), an infectious human pathogen and satellite of hepatitis B virus, leads to intensified disease symptoms, including progression to liver cirrhosis. Both the circular RNA genome of HDV and its complementary antigenome contain the same cis-cleaving catalytic RNA motif that plays a crucial role in virus replication. Previously, the high-resolution crystal structure of the product form of a cis-acting genomic HDV ribozyme has been determined, while a trans-acting version of the ribozyme was used to dissect the cleavage reaction pathway. Using fluorescence resonance energy transfer (FRET) on a synthetic trans-cleaving form of the ribozyme, we are able to directly observe substrate binding (at a rate constant k_{on} of 7.8×10^6 M^{-1} min^{-1} at pH 7.5, 11 mM $MgCl_2$, and 25 °C) and dissociation (at 0.34 min^{-1}). Steady-state and time-resolved FRET experiments in solution and in nondenaturing gels reveal that the substrate (precursor) complex is slightly more compact (by ∼3 Å) than the free ribozyme, yet becomes significantly extended (by ∼15 Å) upon cleavage and product complex formation. We also find that trans cleavage is characterized by a high transition-state entropy (−26 eu). We propose that the significant global conformational change that we observe between the precursor and product structures occurs on the reaction trajectory into a constrained product complex-like transition state. Our observations may present the structural basis of the recently described utilization of intrinsic substrate binding energy to the overall catalytic rate enhancement by the trans-acting HDV ribozyme.

The hepatitis delta virus (HDV)[1] is a human pathogen and satellite of the hepatitis B virus (*1*). Superinfection by HDV leads to intensification of the symptoms of hepatitis B infection and frequent progression to liver cirrhosis (*2*). HDV contains a circular, viroid-like RNA genome of 1679 nucleotides. This genomic RNA undergoes replication via a double rolling-circle mechanism, producing multimers of the genomic and antigenomic RNAs, both of which self-cleave and religate into circular monomers (*1*). The cleavage activity in the genomic and antigenomic RNAs can be mapped to minimal ∼85 nt motifs. The sequences of these two forms of the HDV catalytic RNA, or ribozyme, are ∼75% identical, and they share a secondary structure composed of a nested double pseudoknot (*3*−*5*).

Self-cleavage of the HDV ribozyme occurs as a general base/acid-catalyzed site-specific transesterification reaction and involves nucleophilic attack of the adjacent 2′-hydroxyl group on the scissile phosphodiester, generating 2′,3′-cyclic phosphate and 5′-hydroxyl termini on the 5′ and 3′ products, respectively (*5*). Self-cleaving (or cis-cleaving) derivatives of the HDV ribozyme have been used to study the interplay of structure and function in this catalytic RNA. A crystal structure of the 3′ product of the self-cleaved genomic ribozyme shows O2 and N3 of a specific cytosine, C75 (C76 in the antigenomic form), within hydrogen bonding distance of the 5′ leaving group, suggesting that this nucleobase plays an active role in catalysis (*6*). A C76A mutation in the antigenomic form results in pK_a changes of the self-cleavage reaction consistent with this nucleotide acting as a general base catalyst (*7*). However, the inverted pH dependence of self-cleavage by the genomic ribozyme in the presence of monovalent metal ions supports a mechanism in which C75/76 acts as a general acid catalyst instead (*8*). Although the latter observation might alternatively be explained in part by the pH susceptibility of a three-nucleotide motif unique to the genomic sequence (*9*), there is little doubt that the HDV ribozyme is an example of a growing number of catalytic RNAs in which an RNA side chain actively contributes to transition-state chemistry (*5*, *10*, *11*).

It has been shown that the HDV ribozyme reaction can also be achieved by separation into a trans-acting ribozyme which binds and cleaves an external substrate, thus greatly facilitating studies of its catalytic mechanism (*3*). In particular, Been and co-workers have been able to kinetically characterize substrate binding and dissociation, cleavage, and product release and binding, through elegant steady-state and pre-steady-state cleavage experiments (*12*, *13*). However, up to now it remained unclear what role, if any, conformational changes play in this reaction pathway. Since information about conformations other than the crystallized 3′ product

† This work was supported by NIH Grant GM62357 to N.G.W., a Rackham Merit predoctoral fellowship and NIH molecular biophysics training grant to D.A.H., and a postdoctoral fellowship from the Swiss National Fonds to D.R.

* To whom correspondence should be addressed. Phone: (734) 615-2060. Fax: (734) 647-4865. E-mail: nwalter@umich.edu.

[1] Abbreviations: FRET, fluorescence resonance energy transfer; fwhm, full width at half-maximum; HDV, hepatitis delta virus; NMR, nuclear magnetic resonance.

10.1021/bi011963t CCC: $22.00
Published on Web 12/27/2001

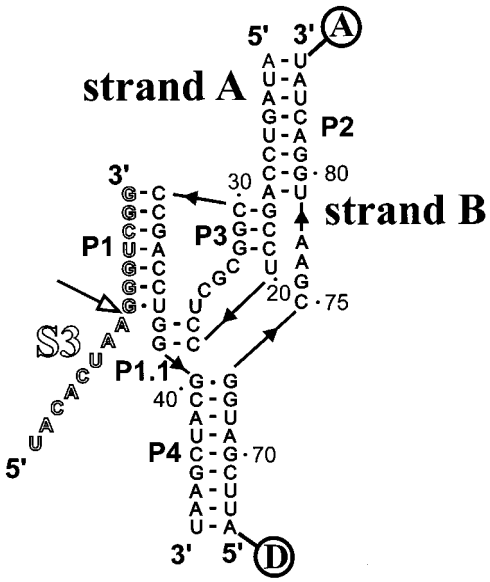

FIGURE 1: Synthetic HDV ribozyme construct D1. The ribozyme portion is shown in bold and consists of two separate RNA strands (A and B). For FRET studies, donor (D, fluorescein) and acceptor (A, tetramethylrhodamine) fluorophores were coupled to the termini of strand B as indicated. Substrate strand S3 is shown outlined. The 3′ product comprises the substrate sequence 3′ of the cleavage site (arrow).

form has been lacking, the prevailing assumption has been that both the precursor and transition-state structures resemble the latter (*6*, *14*).

On the basis of our previous experience with observing ribozyme conformational changes by fluorescence resonance energy transfer (FRET) (*15*−*20*), we have devised FRET assays that study conformational intermediates on the reaction pathway of the trans-acting HDV ribozyme. To this end, we have modified the naturally occurring HDV ribozyme to assemble it from a synthetic substrate and two ribozyme strands (Figure 1). We show here that this three-strand ribozyme version yields cleavage rate constants and metal ion, temperature, and pH dependencies comparable to those of other trans-cleaving HDV ribozymes. In addition, it allows for site-specific incorporation of the donor−acceptor fluorescein−tetramethylrhodamine fluorophore pair at the ends of helices P4 and P2, respectively (Figure 1). Steady-state FRET experiments reveal the kinetics of distinct conformational changes upon substrate binding and cleavage. The observed conformers migrate as homogeneous bands in a FRET gel shift assay, and we have analyzed their donor−acceptor distance distributions by time-resolved FRET. We find that the substrate complex is slightly more compact than the free ribozyme, and that it becomes significantly extended upon cleavage and product complex formation. We discuss these results in light of the most recent studies of catalysis by the HDV ribozyme (reviewed in ref *5*) and propose that the substrate complex undergoes a conformational change on the reaction trajectory toward a product complex-like transition state.

MATERIALS AND METHODS

Preparation of RNA Oligonucleotides. RNA oligonucleotides were purchased from Dhamacon Research, Inc., obtained from the RNA synthesis facility at the University of Vermont (Burlington, VT), or made in-house using standard solid-phase phosphoramidite chemistry (Glen Research). Dharmacon RNA was deprotected as suggested by the manufacturer, while RNA from the other sources was deprotected by a two-step protocol as previously described (*18*). Deprotected RNA was purified by denaturing 20% polyacrylamide, 8 M urea gel electrophoresis, diffusion elution into 0.5 M NH_4OAc, 0.1% SDS, and 0.1 mM EDTA overnight at 4 °C, chloroform extraction, ethanol precipitation, and C_8 reverse-phase HPLC with a linear acetonitrile gradient in triethylammonium acetate as described previously (*18*). For FRET measurements, the three-strand ribozyme (sequences given in Figure 1) was modified on the 5′ and 3′ ends of strand B with fluorescein and tetramethylrhodamine, respectively, as described previously (*18*, *19*). To obtain a chemically blocked, noncleavable substrate analogue for structural analyses, the substrate was modified with a 2′-methoxy group at the cleavage site (Figure 1). The 3′ product had the sequence 5′-GGGUCGG-3′. RNA concentrations were calculated from their absorption at 260 nm and corrected for the additional absorption of fluorescein and tetramethylrhodamine by using the relations $A_{260}/A_{492} = 0.3$ and $A_{260}/A_{554} = 0.49$, respectively.

Cleavage Reactions. The 5′-^{32}P-labeled substrate was prepared by phosphorylation with T4 polynucleotide kinase and [γ-^{32}P]ATP. All cleavage reactions were conducted under single-turnover (pre-steady-state) conditions. Standard conditions were 40 mM Tris-HCl (pH 7.5) and 11 mM $MgCl_2$, at 25 °C, unless otherwise stated. Ribozyme was preannealed from strand A and twice the concentration of strand B in standard buffer, by heating to 70 °C for 2 min and cooling to room temperature. After preincubation for 15 min at 25 °C, a trace (<4 nM) amount of 5′-^{32}P-labeled substrate (also in standard buffer) was added to the ribozyme at a final concentration of 400 nM (based on the strand A concentration), unless otherwise noted. Aliquots (5 μL) were taken at appropriate time intervals and the reactions quenched with 10 μL of 80% formamide, 0.025% xylene cyanol, 0.025% bromophenol blue, and 50 mM EDTA. The 5′ cleavage product was separated from the uncleaved substrate by denaturing 20% polyacrylamide, 8 M urea gel electrophoresis and was quantified and normalized to the sum of the substrate and product bands using a Storm 840 PhosphorImager with ImageQuant software (Molecular Dynamics). Error bars stem from typically three independent cleavage assays. Time traces of product formation were fit to the single-exponential first-order rate equation $y = y_0 + A_1(1 - e^{-t/\tau_1})$, employing Marquardt−Levenberg nonlinear least-squares regression (Microcal Origin), where A_1 is the amplitude and $1/\tau_1$ the pseudo-first-order rate constant k_{obs}. Ribozyme (Rz) and metal ion (M^{2+}) dependencies of this rate constant were fit to the binding equations

$$k_{obs} = k_{cleav}\frac{[Rz]^n}{[Rz]^n + K_M{}^n}$$

and

$$k_{obs} = k_{max}\frac{[M^{2+}]^n}{[M^{2+}]^n + K_{D,app}{}^n}$$

to yield the cleavage rate constant k_{cleav} under standard conditions, the apparent ribozyme and metal ion dissociation constants K_M and $K_{D,app}$, respectively, and a cooperativity coefficient n (*15*). For the pH dependence, cleavage was assayed in a buffer with 25 mM MES, 25 mM acetic acid, and 50 mM Tris (pH 5.0−8.0) or a buffer with 50 mM MES, 25 mM Tris, and 25 mM 2-amino-2-methyl-1-propanol (pH 8.5−9.5) (*7*). The pH-dependent rate constants were fit to the equation $k_{obs} = k_{max}/(1 + 10^{pK_{a1}-pH} + 10^{pH-pK_{a2}})$ (*21*).

Steady-State Fluorescence Measurements. Steady-state FRET measurements of HDV ribozyme doubly labeled with fluorescein and tetramethylrhodamine were performed on an Aminco-Bowman Series 2 (AB2) spectrofluorometer (Spectronic) in a manner similar to that of previously described experiments (*15*, *19*). Annealed ribozyme [final concentration of 50 nM; with an at least 2-fold (saturating) excess of unlabeled strand A] was incubated at 25 °C for at least 15 min in standard buffer supplemented with 25 mM dithiothreitol as a radical quencher, and was then transferred to a 150 μL cuvette. The substrate, noncleavable substrate analogue, or 3′ product was manually added to a (saturating) 5-fold excess, unless otherwise stated. Fluorescein was excited at 490 nm (4 nm bandwidth), and for kinetic experiments, fluorescence emission was recorded simultaneously at the fluorescein (520 nm, 8 nm bandwidth) and tetramethylrhodamine (585 nm, 8 nm bandwidth) wavelengths, by shifting the emission monochromator back and forth. A FRET ratio Q (F_{585}/F_{520}) was calculated and normalized with its starting value to obtain the relative FRET efficiency. The resulting time traces were fit, in a manner similar to that described for the cleavage kinetics, to single- or double-exponential increase and decrease functions of the form $y = y_0 + A_1(1 - e^{-t/\tau}) + ...$ and $y = y_0 + A_1e^{-t/\tau} + ...$, respectively, as required.

To derive fluorescence anisotropies as a measure for fluorophore mobility, the internal film polarizers of the AB2 spectrofluorometer were utilized, and fluorescence intensities at the specific donor and acceptor excitation and emission wavelengths were measured with excitation and emission polarizers subsequently in all four possible combinations of vertical (v, 0°) or horizontal (h, 90°) alignment, I_{vv}, I_{vh}, I_{hv}, and I_{hh}. Anisotropy A was calculated using the following expression (*22*):

$$A = \frac{I_{vv} - gI_{vh}}{I_{vv} + 2gI_{vh}}$$

where $g = I_{hv}/I_{hh}$.

Time-Resolved FRET Measurements. The global structure of the HDV ribozyme was studied by trFRET analysis of ribozyme complexes doubly labeled with fluorescein and tetramethylrhodamine. The annealed ribozyme complexes (150 μL; 1 μM doubly labeled ribozyme strand B, 3 μM strand A, and either 6 μM substrate, noncleavable substrate analogue, or 3′ product) were incubated at 25 °C for at least 15 min in standard buffer, prior to collecting time-resolved emission profiles of the fluorescein donor using time-correlated single-photon counting, which was similar to previously described procedures (*16*). A frequency-doubled Nd:YVO_4 laser (Spectra-Physics Millenia Xs-P, operated at 8.9 W) pumped a frequency-doubled, mode-locked Ti:Sapphire laser (Spectra-Physics Tsunami, operated at 1 W) that excited fluorescein at 490 nm by 2 ps width pulses, picked down to 4 MHz. Isotropic emission detection to >40000 peak counts was performed under magic angle polarizer conditions at 520 nm (10 nm band-pass interference filter). Using a microchannel plate photomultiplier tube (Hamamatsu R3809U-50) feeding into an SPC-630 time-correlated single-photon counting card (Becker & Hickl), decays were collected in 4096 channels with a time increment of 12.20 ps/channel. An instrument response function was measured as the scattering signal from a dilute solution of nondairy coffee creamer to deconvolute the fluorescence decay data. To measure donor−acceptor distances, two time-resolved fluorescence decays were collected, with and without the acceptor in place. The fluorescein emission decay in the donor-only complex was used to extract the two or three intrinsic donor lifetimes τ_i with their fractional contributions α_i by a sum-of-exponentials fit. The data from the doubly labeled complex $I_{DA}(t)$ were then fit with a model for distance distributions

$$I_{DA}(t) = \sum_k f_k \int P_k(R) \sum_i \alpha_i \exp\left\{-\frac{t}{\tau_i}\left[1 + \left(\frac{R_0}{R}\right)^6\right]\right\} dR$$

where the first sum refers to the number of distributions, either one or two, each with a fractional population f_k and a distance distribution $P_k(R)$. Distance distributions were modeled as weighted three-dimensional Gaussian functions

$$P(R) = 4\pi R^2 c \exp[-a(R - b)^2]$$

where a and b are parameters that describe the shape of the distribution and c is a normalization constant. Fitting was performed by nonlinear least-squares regression, with a, b, and f_k for each distribution as adjustable parameters. An additional adjustable parameter was a small fraction of singly labeled complex (always <5%), accounting for the photobleached acceptor fluorophore. The τ_i and α_i values from the donor-only decay were used under the assumption that each intrinsic donor lifetime is influenced independently by the presence of the acceptor at a distance R and is split into a lifetime distribution by the distribution in R.

In all cases, a single distance distribution gave a good fit, as judged by the reduced χ^2 value (<1.5) and by evenly distributed residuals. To extract absolute distances, a value of 55 Å for the Förster distance R_0 of fluorescein and tetramethylrhodamine was used (*16*), and a value of $^2/_3$ was assumed for the orientation factor, based on the high mobility of the fluorophores as is evident from their low fluorescence anisotropies (Table 2) (*18*, *19*).

FRET Gel Shift Assays. Nondenaturing gel electrophoresis was performed in 10% polyacrylamide (19:1 acrylamide:bisacrylamide ratio), 40 mM Tris-HCl (pH 7.5), and 11 mM $Mg(OAc)_2$. Ten pmol of doubly fluorophore-labeled ribozyme strand B was annealed to 20 pmol of strand A by heating for 2 min to 70 °C and cooling to room temperature in 40 mM Tris-HCl (pH 7.5), 11 mM $MgCl_2$, 25 mM DTT, and 10% glycerol. The ribozyme was equilibrated at 25 °C for at least 15 min prior to addition of 50 pmol of substrate, noncleavable substrate analogue, or 3′ product (total volume of 10−20 μL). In the meantime, the assembled electrophoresis unit had been equilibrated to 4 °C for at least 2 h, the samples were then loaded on the gel, and an electric field of

Table 1: Cleavage Rate Constants, Activation Parameters, Metal Ion Dissociation Constants, and pK_as for HDV Ribozyme Construct D1[a]

parameter	substrate S3
k_{cleav} (pH 7.5, 11 mM Mg^{2+}, 25 °C)	0.68 ± 0.08 min^{-1}
E_a	13 ± 1 kcal/mol
$\Delta G^{\ddagger}$	20.1 ± 0.1 kcal/mol
$\Delta H^{\ddagger}$	12 ± 1 kcal/mol
$\Delta S^{\ddagger}$	-26 ± 4 eu
$K_{D,app}(Mg^{2+})$	8 ± 1 mM
$K_{D,app}(Ca^{2+})$	3 ± 1 mM
$K_{D,app}(Mn^{2+})$	5 ± 2 mM
pK_{a1}, pK_{a2}	5.6, 8.9
k_{on}	$(7.8 \pm 0.2) \times 10^6$ M^{-1} min^{-1}
k_{off}	0.34 ± 0.04 min^{-1}

[a] The cleavage rate constant k_{cleav} was determined as described in the text under standard conditions: single turnover, 40 mM Tris-HCl, pH 7.5, 11 mM $MgCl_2$, and 25 °C. Activation parameters were calculated for a T of 298.15 K (25 °C) from the equations $\Delta G^{\ddagger} = -RT \ln(k_{cleav}h/k_BT)$, where R is the gas constant, h is Planck's constant, and k_B is Boltzmann's constant; $\Delta H^{\ddagger} = E_a - RT$, with the activation energy E_a derived from the data in Figure 2c; and $\Delta S^{\ddagger} = (\Delta H^{\ddagger} - \Delta G^{\ddagger})/T$. $K_{D,app}$s were derived from the data in Figures 2b and 3, pK_as from the data in Figure 2d, and k_{on} and k_{off} from the data in panels c and d of Figure 4, respectively, with errors derived from typically three measurements.

Table 2: Fluorescence Properties of Fluorescein- and Tetramethylrhodamine-Labeled Ribozyme Complexes[a]

parameter	D1	D1+ncS3	D1+3′P
anisotropy with fluorescein	0.013 ± 0.003	0.013 ± 0.003	0.013 ± 0.003
anisotropy with tetramethylrhodamine	0.021 ± 0.003	0.024 ± 0.003	0.022 ± 0.003
mean fluorescein lifetime without acceptor (ns)	4.11 ± 0.05	4.18 ± 0.05	3.93 ± 0.05
mean donor−acceptor distance (Å)	56 ± 1	53 ± 1	68 ± 1
fwhm (Å)	25 ± 1	19 ± 1	27 ± 1
χ^2	1.36	1.43	1.48

[a] Fluorescence anisotropies and lifetimes were measured and donor−acceptor distances derived as described in Materials and Methods. χ^2 is the reduced chi-square value.

6 V/cm was immediately applied. After electrophoresis for 36 h, the gel was scanned between its low-fluorescence glass plates in a FluorImager SI fluorescence scanner with ImageQuant software (Molecular Dynamics) as described previously (*23*). Briefly, a 488 nm laser excites the fluorescein, and fluorescence is collected by a fiber optic bundle to be quantified by a photomultiplier tube after passing through either a 530 nm band-pass filter (donor fluorescein) or a 610 nm long-pass filter (acceptor tetramethylrhodamine). RNAs labeled with only fluorescein and only tetramethylrhodamine were included as color calibration standards. From the volume reports, the relative FRET efficiency of selected bands was calculated as $F_{acceptor}/F_{donor}$. Defining the readout of F_{donor} as green and $F_{acceptor}$ as red, we superimposed the corresponding color images using Photoshop 5.5 (Adobe) to generate Figure 5a.

RESULTS

A Synthetic Three-Strand HDV Ribozyme Has Catalytic Properties Similar to Those of Other Trans-Cleaving Ribozymes. To incorporate site-specific fluorophore labels into RNA for structure probing by FRET, synthetic RNA strands have to be used, which are currently limited to ~40−50 nucleotides in length (*19*). Our synthetic trans-acting construct D1, therefore, is composed of ribozyme strands A and B and substrate strand S3 (Figure 1); it was derived after screening a number of variants for optimal activity. The ribozyme is a hybrid between the genomic form [represented in the sequences of helices P2−P4, and J4/2 (the connecting strand between P4 and P2)] and the antigenomic form of the HDV ribozyme [represented in P1, the closing loop of P3, and J1/4 (the connecting strand between P1 and P4)]; substrate S3 shares the eight nucleotides at its 3′ end with the antigenomic HDV ribozyme and has a sequence upstream of the cleavage site that was suggested in an earlier screen for optimal substrates (*24*). In the design of all three RNA strands, we utilized Michael Zuker's RNA folding software "mfold version 3.0" (*25*) to avoid undesired alternate secondary structures. To test the validity of such a construct as a model system, we first characterized its catalytic activity in comparison with previously characterized HDV ribozymes transcribed in vitro.

Under standard single-turnover (pre-steady-state) reaction conditions [trace amounts of radiolabeled substrate and a >10-fold excess of ribozyme in 40 mM Tris-HCl (pH 7.5) and 11 mM $MgCl_2$ at 25 °C (see Materials and Methods)], we varied the ribozyme concentration between 50 and 800 nM (Figure 2a). The observed pseudo-first-order, single-exponential rate constants were plotted as a function of ribozyme concentration and fit to a binding equation, yielding a rate constant for the rate-limiting step of cleavage (k_{cleav}) at 25 °C of 0.68 min^{-1} (Figure 2a inset and Table 1). This rate constant compares well with those of other trans-cleaving HDV ribozymes that range from 0.1 to 0.9 min^{-1}, typically at 37 °C (*3*, *12*, *21*, *24*, *26*).

Next, we measured the cleavage activity of D1 under our standard single-turnover conditions (at 400 nM ribozyme excess) but at increasing Mg^{2+} concentrations (Figure 2b). The observed rate constants increase substantially from 0.035 to 0.82 min^{-1} as the Mg^{2+} concentration increases from 1 to 20 mM, yielding an apparent magnesium dissociation constant of 8 mM (Table 1). The Mg^{2+} affinity of our construct is therefore somewhat lower than that reported for a cis-cleaving HDV ribozyme ($K_{D,app}$ = 1 mM) (*27*), but higher than that of an earlier three-strand ribozyme construct ($K_{D,app}$ = 40 mM) (*26*).

Next, the temperature dependence of cleavage by our D1 ribozyme was measured. Rate constants under standard conditions increase by a factor of 5 between 10 and 37 °C. At 37 °C, the ribozyme cleaves S3 with a rate constant of 0.77 min^{-1}, comparable to that reported for other trans-cleaving HDV ribozymes under similar conditions [e.g., 0.91 min^{-1} (*12*)]. When using Arrhenius analysis, we obtain an activation energy E_a of 13 kcal/mol (Figure 2c and Table 1). The slight deviation from linearity at a higher temperature (37 °C; leftmost data point in Figure 2c) may indicate a beginning change in the rate-limiting step, possibly due to a different partitioning of the substrate between cleavage and dissociation. A similar decrease in activity at temperatures around 40 °C was observed for a previous three-strand HDV ribozyme (*26*), while some cis-cleaving HDV ribozymes are reactive up to temperatures as high as 80 °C (*4*, *28*, *29*).

From E_a and k_{cleav}, activation parameters were calculated which reflect differences between the ground and transition

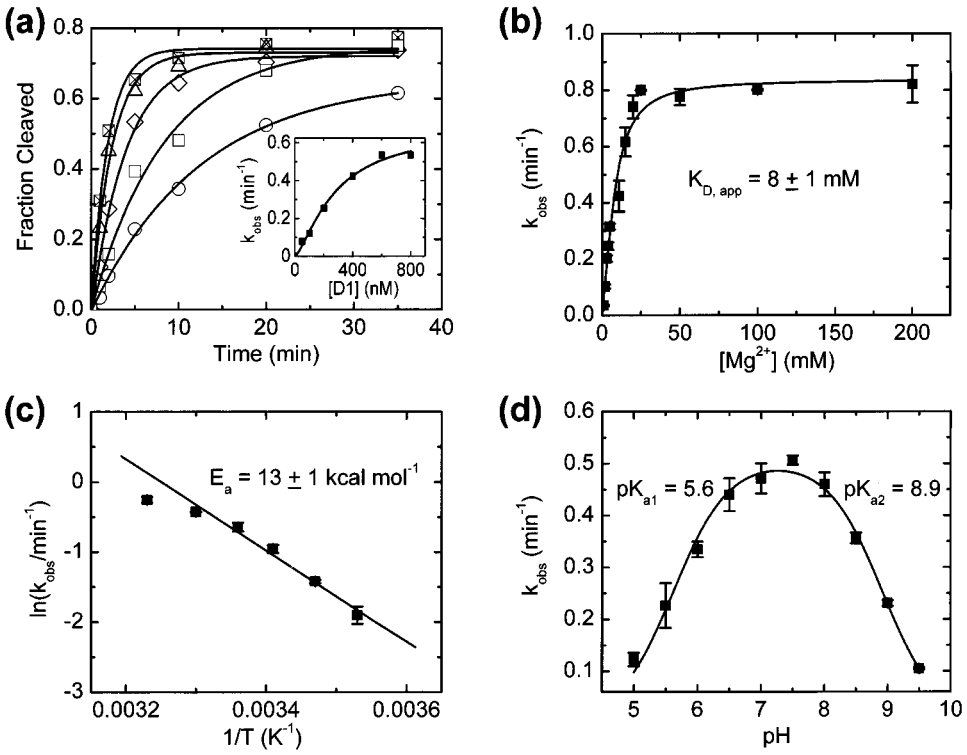

FIGURE 2: Cleavage of substrate S3 by construct D1 under single-turnover conditions. (a) Cleavage time courses under standard conditions of 40 mM Tris-HCl (pH 7.5) and 11 mM $MgCl_2$ at 25 °C with varying ribozyme concentrations [(○) 50, (□) 100, (◇) 200, (△) 400, and (crossed box) 800 nM]. Data were fit to a single-exponential increase function (—) to yield the rate constants k_{obs} reported in the inset (total fraction cleaved of typically 77%). The inset shows the dependence of k_{obs} on ribozyme concentration which was fit to a binding equation (—; see Materials and Methods), yielding a k_{cleav} of 0.68 min^{-1} (K_M = 280 nM). (b) Observed cleavage rate constants k_{obs} as a function of Mg^{2+} concentration. The data were fit to a cooperative binding equation (—, cooperativity coefficient n = 1.6; see Materials and Methods) to yield the apparent Mg^{2+} dissociation constant $K_{D,app}$. (c) Temperature dependence of the observed cleavage rate constants. Linear regression in this Arrhenius plot (—) yields the activation energy E_a. (d) pH dependence of the observed cleavage rate constants. The data were fit (—; see Materials and Methods) to yield two pK_a values.

states (Table 1). The activation Gibbs energy $\Delta G^{\ddagger}$ at 25 °C for S3 cleavage is 20.1 kcal/mol; the activation enthalpy $\Delta H^{\ddagger}$ is 12 kcal/mol, and the activation entropy $\Delta S^{\ddagger}$ is highly unfavorable (as discussed below), with a value of −26 eu (Table 1).

pH profiles have played a key role in the discovery that C75/76 is a catalytic residue in the HDV ribozyme, as log-linear relationships of rate constant and pH are commonly interpreted as reflecting the fact that reaction chemistry is rate-limiting (*7*, *8*). To verify that our D1 ribozyme utilizes the same reaction pathway as other HDV ribozymes, we studied the pH dependence of cleavage. Indeed, the pH profile has a similar bell shape (Figure 2d) like that of previously characterized trans-acting (*21*) and cis-acting HDV ribozymes (*9*). From the pH dependence, two pK_as of 5.6 and 8.9 are derived (Figure 2d and Table 1). These values are identical, within experimental error (±0.1), with those of another trans-acting HDV ribozyme that exhibits pK_{a1} and pK_{a2} values of 5.7 and 8.9, respectively (*21*). We note that these pH profiles suggest that a pH-dependent step is rate-limiting for our D1 construct at low pH (below pK_{a1}) (*5*, *30*), as well as a second one at high pH (above pK_{a2}). Interestingly, the pK_{a1} reported for cis-acting genomic and antigenomic HDV ribozymes is 0.5 pH unit higher at pH 6.1 (*7*−*9*).

The Three-Strand HDV Ribozyme Is Active in the Presence of Calcium and Manganese, but Not Monovalent Cations. Besides Mg^{2+}, calcium and manganese have been found to activate the HDV ribozyme (*21*, *27*, *31*, *32*). To further evaluate our D1 construct, we performed cleavage assays in the presence of increasing concentrations of either Ca^{2+} or Mn^{2+}.

Under standard conditions, the cleavage rate constant increases from 0.03 to 0.13 min^{-1} between 1 and 125 mM Ca^{2+} (Figure 3a). This is noticeably slower than for a trans-cleaving two-strand HDV ribozyme that yielded a 60% faster cleavage rate in Ca^{2+} than in Mg^{2+} (*21*). However, our apparent Ca^{2+} dissociation constant of 3 mM suggests a 2−3-fold tighter binding of Ca^{2+} than of Mg^{2+} (Table 1).

Between 1 and 15 mM Mn^{2+}, the cleavage rate constant of S3 increases from 0.05 to 0.25 min^{-1} (Figure 3b). The apparent Mn^{2+} dissociation constant is 5 mM (Table 1), similar to those of other trans-acting HDV ribozymes (*21*). Finally, we tested our D1 ribozyme in 1 M Na^{+}, but were unable to detect any cleavage activity at either pH 7.5 or 5.5 (data not shown). Activity in the presence of monovalent cations at low pH has been observed for a cis-acting ribozyme derived from the genomic sequence (*8*), yet it has been absent from other HDV ribozymes that, like our construct, lack a specific three-nucleotide CAA insert between P1.1 and P4 (*9*, *20*).

In summary, our three-strand synthetic D1 ribozyme behaves like previously characterized trans-acting constructs and therefore proves to be a valid model system for probing the conformational dynamics of the HDV ribozyme, by applying site-specifically incorporated fluorophores (*19*).

Steady-State FRET Assays Reveal Differences between Pre- and Postcleavage Structures and Report on the Folding

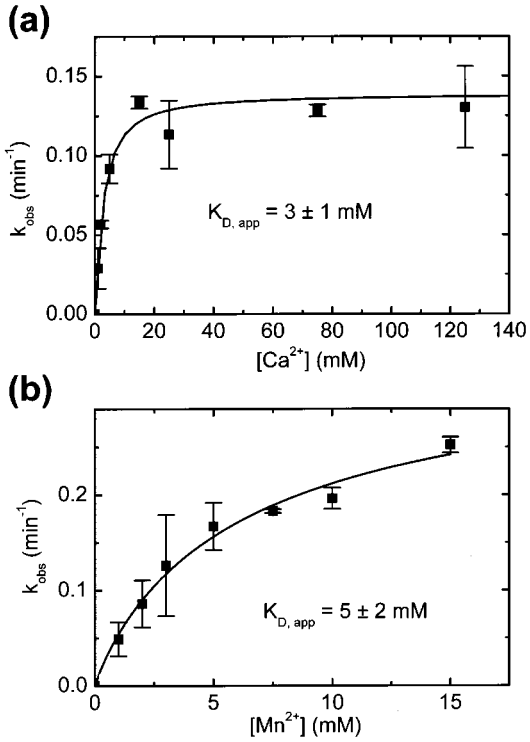

FIGURE 3: Effect of Ca^{2+} and Mn^{2+} on the observed cleavage rate constant k_{obs} in 40 mM Tris-HCl (pH 7.5) at 25 °C. (a) Ca^{2+} dependence of cleavage. Fitting to a cooperative binding equation (—, cooperativity coefficient $n = 1.2$; see Materials and Methods) yields the apparent dissociation constant $K_{D,app}$ for Ca^{2+}. (b) Mn^{2+} dependence of cleavage. The fit to a cooperative binding equation (—, cooperativity coefficient $n = 0.9$; see Materials and Methods) yields the apparent dissociation constant $K_{D,app}$ for Mn^{2+}.

Kinetics of the HDV Ribozyme. We utilized fluorescence resonance energy transfer (FRET) between a donor and acceptor fluorophore to probe conformational changes on the reaction pathway of the HDV ribozyme. FRET is highly distance-dependent and therefore sensitive to changes in fluorophore distance as a result of global structural changes of the RNA that is being studied (*18*, *19*). Strand B of our D1 construct was labeled with a 5′ fluorescein and 3′ tetramethylrhodamine donor−acceptor pair (Figure 1). Cleavage assays comparing the labeled with the unlabeled D1 construct gave similar rate constants and extents of cleavage (data not shown), demonstrating that the fluorophores, far distant from the catalytic core, do not significantly alter the catalytic behavior. In all fluorescence assays, an at least 2-fold excess of the unlabeled A and substrate strands was added under standard conditions (see Materials and Methods) to ensure saturation of the labeled strand B.

The fluorescence spectrum of the assembled ribozyme is shown in Figure 4a. It is characterized by the two emission peaks expected for fluorescein and tetramethylrhodamine, with maxima at 520 and 585 nm, respectively. Addition of a saturating excess of a chemically blocked, noncleavable substrate analogue of S3 (termed ncS3) leads to a slight yet significant decrease in fluorescein (donor) and increase in tetramethylrhodamine (acceptor) fluorescence (Figure 4a). In contrast, addition of saturating concentrations of just the 3′ product portion of this substrate [termed 3′P (5′-GGGUCGG-3′ sequence); see Figure 1] yields a strong increase in fluorescein and decrease in tetramethylrhodamine emission (Figure 4a). Thus, while the ribozyme−substrate complex shows a slight increase in the level of energy transfer from donor to acceptor (or decrease in their distance) compared to the free ribozyme, the ribozyme−3′ product complex shows a significant decrease in the level of FRET (or increase in fluorophore distance). Similar results were obtained with other closely related substrates and when the donor and acceptor were coupled to the 5′ and 3′ ends of strand A, respectively (data not shown).

These results are corroborated by time courses taken upon addition of ncS3, S3, or 3′P. When saturating concentrations of ncS3 were added to the ribozyme, the relative FRET efficiency increased by 9% (Figure 4b). The pseudo-first-order rate constant for this increase is linearly dependent on the excess concentration of ncS3, indicating that the observed increase in the level of FRET is a direct result of substrate binding. From this dependence, we were able to extract a second-order substrate binding rate constant k_{on} of 7.8×10^6 M^{-1} min^{-1} (Figure 4c and Table 1), which is within 3-fold of a value previously measured for a related HDV ribozyme−substrate complex (*12*).

In contrast, when adding a saturating concentration of 3′P to the ribozyme, we observed a fast (slightly double-exponential) decrease in relative FRET efficiency of 33% (Figure 4b). We estimate the rate constant to be approximately 11 min^{-1} at 250 nM 3′P. This rate constant is dependent on the product concentration and therefore appears to reflect product binding (data not shown).

Next, we added a saturating excess of cleavable substrate S3 to the ribozyme. First, a brief and subtle increase in the relative FRET efficiency is observed, presumably a result of formation of a ribozyme−substrate complex (inset of Figure 4b). Upon substrate cleavage, which leads to rapid dissociation of its 5′ portion (*12*) and formation of the ribozyme−3′ product complex, a decrease in relative FRET efficiency is observed with a rate constant of 0.50 min^{-1} (Figure 4b). This value is close to the one measured in our single-turnover cleavage assays (Table 1). In addition, the overall decrease in relative FRET efficiency of ∼26% over the course of 30 min is consistent with the 33% FRET efficiency decrease from direct formation of the ribozyme−3′ product complex, as ∼77% of the S3 is typically cleaved during this time (Figure 2a). These observations imply that the 3′ product stays bound, i.e., is not replaced by excess substrate, a notion consistent with previous findings (*12*).

A recent study by Shih and Been (*12*) reported that the 3′ product has a dissociation rate constant that is ∼240 times slower than that of the substrate. This makes 3′P a good chase for probing the dissociation rate constant of the noncleavable substrate analogue ncS3. To this end, we first formed the ribozyme−ncS3 complex, and then added 2 μM 3′P. We observed a single-exponential FRET efficiency decrease (Figure 4d). Its rate constant k_{off} of 0.34 min^{-1} is independent of the concentration of 3′P (inset of Figure 4d), indicating that our chase concentration is sufficient, and that active displacement (i.e., a promotion of substrate dissociation) by the chase does not take place (*33*). This substrate dissociation rate constant is within 4-fold of a previously reported value for another trans-acting HDV ribozyme (*12*) and, together with the substrate binding rate constant k_{on}, defines the equilibrium dissociation constant K_D ($=k_{off}/k_{on}$) which equals 44 nM. Conversely, the 3′ product could not be chased off its complex, even when utilizing an up to 5 μM excess of

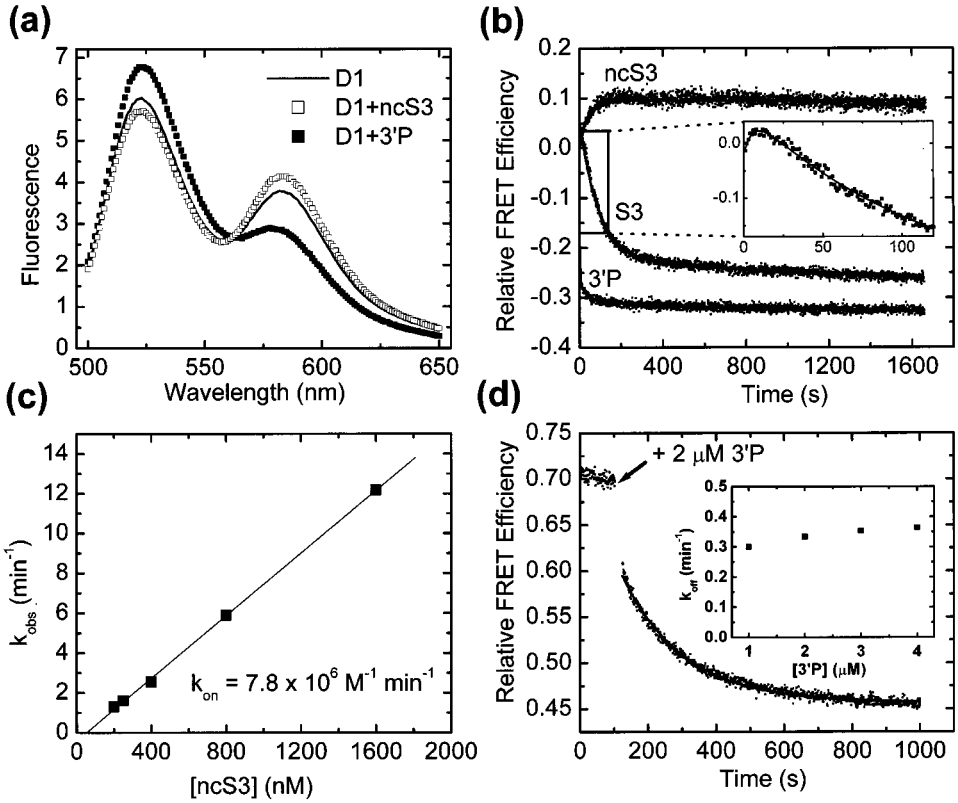

FIGURE 4: Steady-state FRET studies using 50 nM fluorescein- and tetramethylrhodamine-labeled D1 ribozyme in 40 mM Tris-HCl (pH 7.5), 11 mM $MgCl_2$, and 25 mM DTT at 25 °C. (a) Fluorescence emission spectra of the free ribozyme (D1), the ribozyme−noncleavable substrate analogue complex (D1+ncS3), and the ribozyme−3′ product complex (D1+3′P), as indicated. The spectra are scaled to the same fluorophore concentration. Fluorescein was excited at 490 nm, and the curves are the average of five spectra from the same solution. (b) Change over time in the relative FRET efficiency of the doubly labeled ribozyme upon addition of 250 nM noncleavable substrate analogue (ncS3), cleavable substrate (S3), or 3′ product (3′P), as indicated. The data set for ncS3 was fit with a single-exponential increase function (—) to yield a rate constant of 1.61 min^{-1} (amplitude of 0.09) that is reported in panel c. The data set for S3, after a short initial increase, gave a simple exponential decrease that pertains to substrate cleavage [inset (—); decrease rate constant of 0.50 min^{-1}]. The 3′P data set decreases double exponentially (see the text). (c) Concentration dependence of the observed pseudo-first-order rate constant upon addition of excess ncS3 to the ribozyme. The slope of the linear regression line reveals the bimolecular binding rate constant k_{on}. (d) Dissociation of the noncleavable substrate analogue from its ribozyme complex. The ribozyme−ncS3 complex (50 nM, with a 200 nM excess of ncS3) was chased with 2 μM 3′ product, and the resulting decrease in the FRET ratio Q was fit to a single-exponential decrease function to yield a dissociation constant k_{off} of 0.34 min^{-1} (—). There is no significant dependence on the chase concentration (inset).

ncS3 as a chase (data not shown), indicating its significantly higher binding affinity.

In summary, these FRET data are consistent with a decrease in fluorophore distance (higher FRET efficiency) upon substrate binding, and an increase in their distance (lower FRET efficiency) upon substrate cleavage, revealing structural distinctions between the substrate and 3′ product complexes.

A FRET Gel Shift Assay Demonstrates the Homogeneity of the Various, Structurally Distinct Ribozyme Complexes. To test the homogeneity of our preparations and confirm that the ribozyme−substrate and −product complexes are indeed structurally distinct, we developed a mobility shift assay in which we analyzed the relative FRET efficiencies of the doubly labeled ribozyme complexes after electrophoresis in nondenaturing polyacrylamide gels (see Materials and Methods). We found that the free ribozyme (D1), the ribozyme−3′ product complex (D1+3′P), and the ribozyme−noncleavable substrate analogue complex (D1+ncS3) all migrate as homogeneous single bands (Figure 5a). Any alternate bands had less than 15% of the intensity of the major ones (data not shown). Consistent with our solution FRET assays, the ribozyme (D1) lane shows an intermediate acceptor-to-donor fluorescence (FRET) ratio (Figure 5a, bottom panel). Its band comigrates with the ribozyme−3′P complex that shows a decreased FRET ratio (or "green-shifted", i.e., donor fluorescence-dominated band). Again consistent with the fluorescence measurements, the ribozyme−ncS3 complex has an increased FRET ratio (or "red-shifted", i.e., acceptor fluorescence-dominated band), and its mobility is the lowest. These findings further support the existence of structurally distinct pre- and post-cleavage ribozyme complexes.

In the lane loaded with the ribozyme−cleavable substrate complex (D1+S3), a band identical to the ribozyme−3′P complex is observed, suggesting that the substrate has been largely cleaved and converted into ribozyme-bound 3′ product (Figure 5a). The result is similar when ribozyme is first run into the gel for 2 h, followed by the faster migrating substrate, so that the ribozyme−substrate complex can only form and cleave in the gel (data not shown). These observations provide evidence that cleavage of substrate S3 occurs within the native gel; hence, the ribozyme−substrate complex is catalytically active.

Distances of the Fluorophores in the Ribozyme Complexes Are Revealed by Time-Resolved FRET. While analyses of acceptor-to-donor fluorescence ratios reveal qualitative changes in fluorophore distance, we were also interested in quantifying the underlying RNA structural changes. The decrease in

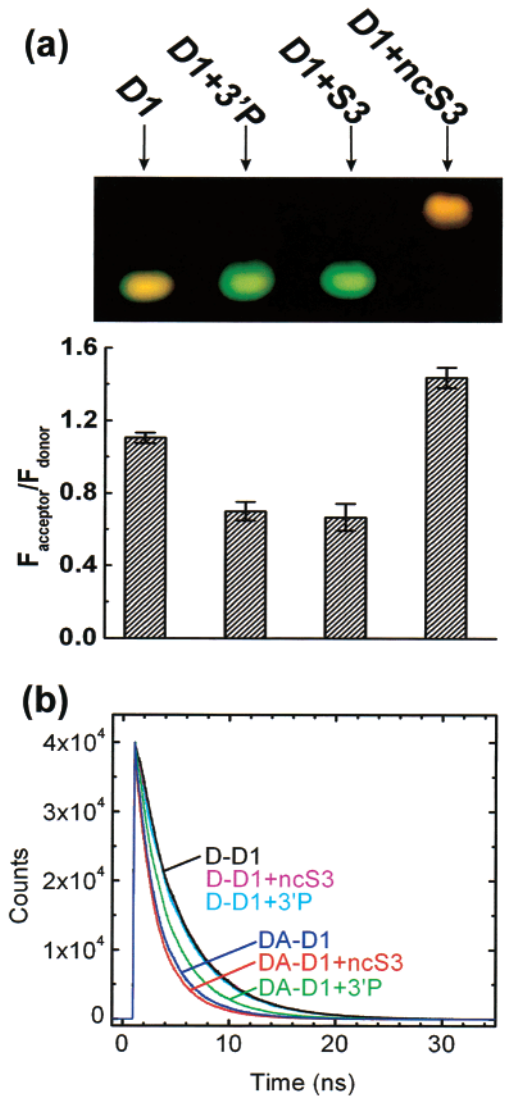

FIGURE 5: Further FRET analysis of D1 ribozyme complexes in 40 mM Tris-HCl (pH 7.5), 11 mM $MgCl_2$, and 25 mM DTT at 25 °C. (a) Nondenaturing gel electrophoresis of fluorescein- and tetramethylrhodamine-labeled complexes (see Materials and Methods). The free ribozyme (D1) comigrates with the ribozyme−3′ product complex (D1+3′P, top panel), but can be distinguished by its ratio of acceptor:donor fluorescence (bottom panel; error bars were derived from three independent gel runs). The ribozyme−substrate complex (D1+S3) undergoes catalysis and is observed as the ribozyme−3′ product complex, while the ribozyme−noncleavable substrate analogue complex (D1+ncS3) stays intact, migrating slower with a higher acceptor:donor fluorescence ratio. (b) Time-resolved FRET analysis (see Materials and Methods). The donor fluorescence decays of the complexes labeled with donor only (D) are contrasted with those of the donor−acceptor (DA) doubly labeled complexes. The ribozyme−noncleavable substrate analogue complex (D1+ncS3) has the fastest decay, followed by the free ribozyme (D1), the ribozyme−3′ product complex (D1+3′P), and the complexes labeled with donor only. The decays were analyzed to yield the mean donor−acceptor distances reported in Table 2. They are shown here normalized to a peak count of 40 000.

donor lifetime upon introduction of the acceptor allows for the measurement of their distance (*18*, *19*). We therefore analyzed the time-resolved donor (fluorescein) decay curves for the ribozyme alone, the ribozyme−noncleavable substrate analogue complex, and the ribozyme−3′ product complex, each of them singly labeled with donor as well as doubly labeled with donor and acceptor (Figure 5b). The decay curves of the three complexes labeled with donor only virtually superimpose and yield similar mean lifetimes between 3.93 and 4.18 ns (Table 2).

As expected, the donor fluorescence decays of all three donor−acceptor doubly labeled complexes are faster, with the ribozyme−ncS3 complex being the fastest, followed by the ribozyme and the ribozyme−3′P complexes (Figure 5b). The anisotropies of the fluorophores in all complexes are low and only slightly vary between the different complexes (Table 2), suggesting that both donor and acceptor can freely rotate. Under this assumption and using Förster theory, the fluorophore distance distributions were analyzed (see Materials and Methods), yielding mean donor−acceptor distances of 56 Å [full width at half-maximum (fwhm) of 25 Å] for the ribozyme, 53 Å (fwhm of 19 Å) for the ribozyme−ncS3 complex, and 68 Å (fwhm of 27 Å) for the ribozyme−3′P complex (Table 2). In all three cases, a single distance distribution fits the decay data well, as judged by the residuals and the reduced χ^2 values (<1.5, Table 2); introducing a second distance distribution does not improve the fits, indicating a high degree of structural homogeneity of our preparations. These time-resolved FRET data confirm our steady-state fluorescence measurements in that the substrate complex is slightly more compact (by ~3 Å) than the free ribozyme, yet becomes significantly extended (by ~15 Å) upon cleavage and product complex formation.

DISCUSSION

We have shown by fluorescence resonance energy transfer that a synthetic trans-acting HDV ribozyme undergoes a global conformational change upon substrate binding and cleavage. This is in contrast to the previous assumption that the precursor, transition state, and cleaved structures are all alike (*6*, *14*) and opens up a discussion on the role of conformational changes in HDV ribozyme catalysis. Comparison of the catalytic behavior, including metal ion, temperature, and pH dependencies, of our construct with that of previously characterized ribozymes suggests that our ribozyme indeed represents features of HDV ribozymes in general. Specifically, its identical bell-shaped pH profile (Figure 2d) suggests that the rate-limiting steps of catalysis throughout the accessible pH range are the same as for other trans-acting ribozymes (*21*).

Figure 6 summarizes our results in a refined reaction pathway of the trans-acting HDV ribozyme. First, steady-state and time-resolved FRET techniques reveal that a noncleavable substrate analogue is bound with a rate constant k_{on} of 7.8×10^6 M^{-1} min^{-1} under standard conditions (pH 7.5, 11 mM $MgCl_2$, 25 °C), upon which the distance between fluorophores at the ends of ribozyme helices P2 and P4 decreases by ~3 Å. This distance change is very modest, but consistently observed as a relative change between the free ribozyme and its substrate complex in steady-state and time-resolved fluorescence experiments both in solution and in nondenaturing polyacrylamide gels. Since neither the free ribozyme nor precleavage ribozyme−substrate structures have yet been characterized by high-resolution techniques, our findings cannot be interpreted in the context of atomic resolution structures. However, it is tempting to speculate that the formation of helix P1 slightly shortens the substrate-binding region of the ribozyme, and/or that the introduction of a helical twist leads to an angular displacement of the

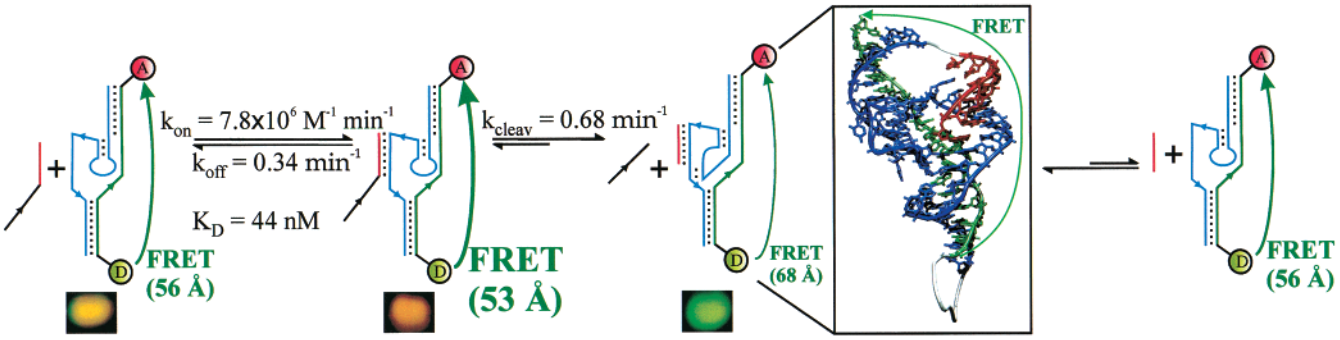

FIGURE 6: Schematic diagram of the minimal reaction mechanism of the trans-acting HDV ribozyme as refined by our studies. Reversible substrate binding and formation of helix P1 cause the ribozyme complex to become slightly more compact; the level og FRET (arrow) between a terminal donor (D) and acceptor (A) fluorophore pair increases, and we observe a single red-shifted band on a FRET gel shift assay (shown below the schematic of the complex). After catalysis, the 5′ product is released (with no observable religation) and the overall structure of the ribozyme−3′ product complex becomes significantly extended as evidenced by an decrease in the level of FRET and a green-shifted FRET gel shift band. This ribozyme−3′ product complex models the postcleavage crystal structure [inset, colored in red (3′ product), blue (ribozyme strand A), and green (strand B); image created with VMD 1.6]. Slow 3′ product release allows the ribozyme to regenerate and undergo another catalytic cycle. One possible explanation for the structural difference between the substrate and product complexes is that helix P1.1, which forms the bottom of the catalytic cleft, may be present in the product, but not the substrate complex, as indicated. The indicated rate and equilibrium constants were measured in 40 mM Tris-HCl (pH 7.5) and 11 mM $MgCl_2$ at 25 °C.

donor−acceptor pair, resulting in the observed subtle decrease in their mean distance. Further studies are needed to clarify this point.

In addition, we were able to directly observe by FRET the dissociation of ribozyme−noncleavable substrate analogue complex at a rate constant k_{off} of 0.34 min^{-1}, yielding an equilibrium dissociation constant K_D (k_{off}/k_{on}) of 44 nM (Figure 6). These binding and dissociation rate and equilibrium constants are close to those in a related trans-acting HDV ribozyme (sharing the same sequence in the substrate-binding helix P1, Figure 1) that were obtained indirectly from pre-steady-state substrate cleavage kinetics ($k_{on} = 2.1 \times 10^7$ M^{-1} min^{-1}, $k_{off} = 1.4$ min^{-1}, and $K_D = 58$ nM, at pH 8, 11 mM $MgCl_2$, and 37 °C) (*12*). It should be noted that, with the cleavable substrate, the binary complex will not reach equilibrium with free ribozyme and substrate prior to cleavage, since the substrate dissociation (0.34 min^{-1}) and cleavage steps (0.68 min^{-1}) have similar rates, as noted previously (*12*).

Second, our FRET experiments show that the end-to-end distance between helices P2 and P4 significantly increases by ~15 Å upon substrate cleavage, 5′ product release, and formation of the ribozyme−3′ product complex. Inspection of the cis-acting, self-cleaved 3′ product crystal structure (*6*) yields an analogous distance of ~74 Å, in reasonable agreement with our measurement of 68 Å, despite sequence differences in helices P2 and P4. The FRET time trace in Figure 4b is consistent with the idea that the cleavable substrate is first bound to a complex with a decreased fluorophore distance, just as the noncleavable substrate analogue is; in a subsequent kinetic step, cleavage and relaxation into the extended conformation of the product complex occur. This observation, together with our time-resolved FRET and FRET gel shift data of the isolated complexes, supports the idea that the more compact structure observed for the noncleavable substrate analogue also forms with the cleavable substrate, and that this is likely the catalytically active structure. Our experiments do not reveal, however, whether the conformational change that accompanies product complex formation is simultaneous with, prior to, or after substrate cleavage. In other words, FRET does not illuminate whether the cleavage transition state structurally resembles the substrate or the product complex, or is structurally distinct from either one.

This latter question directly relates to our understanding of catalysis by the HDV ribozyme. There is strong evidence from pH titration experiments that C75/76 deprotonates the 2′-hydroxyl nucleophile (*7*) and/or protonates the 5′-oxyanion leaving group in the rate-limiting step (i.e., in the transition state) of transesterification (*8*−*10*). In the 3′ product crystal structure, O2 and N3 of C75/76 are within hydrogen bonding distance of the 5′-OH leaving group (*5*, *6*). Therefore, it is plausible that a C75/76−5′-OH hydrogen bond, or a similar interaction, is also present in the transition state, juxtaposing the catalytic base and the scissile phosphate. Given that the substrate and product complexes are structurally distinct, as directly observed here by FRET, we propose that the transition state in HDV ribozyme catalysis is closer in structure to, although not necessarily identical with, the product complex.

Interestingly, Doudna and co-workers have been unable to detect, by site-specific ^{13}C NMR probing of the ground-state substrate and product complexes, the substantial pK_a shift that is observed for the catalytic C75/76 in the transition state (*34*). This result suggests structural and electrostatic differences in the local environment of C75/76 in the transition state compared to both the precursor and product forms of the HDV ribozyme, and is consistent with our capture of significant structural change along the reaction trajectory.

Why is the substrate complex structurally distinct from the product complex and presumably the transition state? Been and co-workers (*12*) have shown that the substrate binds to the trans-acting ribozyme with significantly lower affinity than the 3′ product, a fact that we confirmed and utilized in our FRET-based measurement of the substrate dissociation rate constant. Inspection of the 3′ product crystal structure of the cis-acting ribozyme reveals that the 5′-hydroxyl leaving group is deeply buried in the catalytic cleft, surrounded by C75/76 and helices P1 and P1.1 (*6*) (Figures

1 and 6). The continuous stack of P1, P1.1, and P4 undoubtedly contributes to the high thermodynamic stability of the 3′ product structure. However, it is difficult to imagine how a 5′ extension of the 3′ product could thread out of this compact core without sterical clash. Such an extension may, for example, require a substantial change in substrate backbone trajectory (*5*) and/or breaking of base pairs or stacking interactions in helix P1 or P1.1 (as suggested in Figure 6). FRET does not provide direct insight into the nature of these structural differences between the pre- and postcleavage complexes. However, local structural rearrangements may be substantial considering the significant global structural change evidenced by FRET.

Been and co-workers have recently characterized in more detail the substantial ground-state destabilization of the ribozyme−substrate versus the ribozyme−3′ product complex (*13*). In particular, they examined dependence on length and composition of the substrate sequence 5′ to the cleavage site, for which there is no evidence that it directly interacts with the ribozyme (*5*). The authors conclude that destabilization of substrate binding contributes ∼2 kcal/mol to the overall reduction of 8.5 kcal/mol in the activation free energy of RNA cleavage by the HDV ribozyme. Destabilized substrate binding may be evidence of an energetically unfavorable bend in the substrate or structural disruption in an RNA helix, as invoked above. It seems plausible that the conformational change upon cleavage observed here by FRET may be evidence of the mechanism by which intrinsic substrate binding energy is applied to catalysis. That is, access to the transition state may be controlled by the probability with which a substrate transiently adopts a distinct 3′ product complex-like conformation, in which intrinsic substrate binding interactions are broken. The nontrivial dependence of catalytic activity on the identity of the four nucleotides immediately 5′ to the cleavage site (*13*, *24*) then may be explained by the extent to which these interactions are already disrupted in the ground state. In other words, distinct sequences 5′ to the cleavage site may differ in their flexibility and/or probability to break intrinsic hydrogen bonding and stacking interactions as required to gain access to the 3′ product-like transition state.

In light of this notion, a relevant observation made here is the highly negative cleavage transition-state entropy of −26 eu (Table 1). This value suggests a more strongly constrained (less dynamic) transition state than is observed, e.g., for the hairpin (*17*) or hammerhead ribozymes (*35*) that catalyze a similar transesterification reaction. A constrained transition state is consistent with the idea that catalysis is rate-limited by the probability of a substrate adopting a particular conformation that correctly positions the scissile phosphate in the densely packed catalytic cleft near C75/76.

The same reasoning may explain the observation that trans-cleaving ribozyme constructs such as the one used in this study are consistently ∼10-fold slower in catalysis than cis-cleaving versions (*5*, *12*). The ribozyme−3′ product crystal structure shows that positioning of the 5′-hydroxyl leaving group is facilitated by the helical crossover at the top of helix P1 (Figure 6) (*6*), which is typically absent from trans-cleaving ribozymes. A slower cleavage rate of trans-acting constructs may therefore be explained by a lower probability of adopting the constrained 3′ product complex-like transition-state structure. Such a conformational change may be expected to be pH-independent, although recently pH-dependent RNA conformational changes have been found (*9*). The pH dependence of our construct at low pH suggests that chemistry, and/or a pH-dependent conformational change, is rate-limiting for catalysis under these conditions, as was concluded for cis-acting HDV ribozymes (*7*, *8*). However, the shift in pK_a from 6.1 ± 0.1 for cis-acting ribozymes to 5.6 ± 0.1 for trans-acting ribozymes is consistent with a pH-independent conformational change becoming rate-limiting for trans-cleaving ribozymes at pH >5.6. Alternatively, the transition-state pK_a shift toward neutrality of C75/76 may be less pronounced in trans-acting HDV ribozymes.

In summary, our results improve the understanding of HDV ribozyme catalysis by uncovering a conformational change upon cleavage of a substrate in trans. Our data lead to the proposal of a structural relationship between the transition state and the 3′ product rather than the distinct substrate complex. They also provide a structural rationale for the mechanism by which the HDV ribozyme may utilize intrinsic substrate binding energy to lower the activation barrier of catalysis. Further investigations are currently underway to support this hypothesis.

ACKNOWLEDGMENT

We thank Ken Rodriguez, Diane Hannemann, and Jue Shi for help with the FRET assays, other members of the Walter group for stimulating discussions, Vladimir Ramirez-Carrozzi and Tom Kerppola for making their FluorImager and expertise on gelFRET assays available to us, Steve Parus for help with setting up our laser-induced time-resolved fluorometer, and Bill Gundlach and Gary Glick for some RNA synthesis.

REFERENCES

1. Lai, M. M. (1995) *Annu. Rev. Biochem. 64*, 259−286.
2. Hadziyannis, S. J. (1997) *J. Gastroenterol. Hepatol. 12*, 289−298.
3. Been, M. D., and Wickham, G. S. (1997) *Eur. J. Biochem. 247*, 741−753.
4. Doherty, E. A., and Doudna, J. A. (2000) *Annu. Rev. Biochem. 69*, 597−615.
5. Shih, I. H., and Been, M. D. (2002) *Annu. Rev. Biochem.* (in press).
6. Ferre-D'Amare, A. R., Zhou, K., and Doudna, J. A. (1998) *Nature 395*, 567−574.
7. Perrotta, A. T., Shih, I., and Been, M. D. (1999) *Science 286*, 123−126.
8. Nakano, S., Chadalavada, D. M., and Bevilacqua, P. C. (2000) *Science 287*, 1493−1497.
9. Wadkins, T. S., Shih, I., Perrotta, A. T., and Been, M. D. (2001) *J. Mol. Biol. 305*, 1045−1055.
10. Shih, I. H., and Been, M. D. (2001) *Proc. Natl. Acad. Sci. U.S.A. 98*, 1489−1494.
11. Nakano, S., Proctor, D. J., and Bevilacqua, P. C. (2001) *Biochemistry 40*, 12022−12038.
12. Shih, I., and Been, M. D. (2000) *Biochemistry 39*, 9055−9066.
13. Shih, I., and Been, M. D. (2001) *EMBO J. 20*, 4884−4891.
14. Ferre-D'Amare, A. R., and Doudna, J. A. (2000) *J. Mol. Biol. 295*, 541−556.
15. Walter, N. G., Hampel, K. J., Brown, K. M., and Burke, J. M. (1998) *EMBO J. 17*, 2378−2391.
16. Walter, N. G., Burke, J. M., and Millar, D. P. (1999) *Nat. Struct. Biol. 6*, 544−549.
17. Walter, N. G., Chan, P. A., Hampel, K. J., Millar, D. P., and Burke, J. M. (2001) *Biochemistry 40*, 2580−2587.

18. Walter, N. G., and Burke, J. M. (2000) *Methods Enzymol. 317*, 409−440.
19. Walter, N. G. (2001) *Methods 25*, 19−30.
20. Murray, J. B., Seyhan, A. A., Walter, N. G., Burke, J. M., and Scott, W. G. (1998) *Chem. Biol. 5*, 587−595.
21. Shih, I. H., and Been, M. D. (1999) *RNA 5*, 1140−1148.
22. Lakowicz, J. R. (1999) *Principles of Fluorescence Spectroscopy*, 2nd ed., Kluwer Academic Publishers, New York.
23. Ramirez-Carrozzi, V. R., and Kerppola, T. K. (2001) *Methods 25*, 31−43.
24. Deschenes, P., Lafontaine, D. A., Charland, S., and Perreault, J. P. (2000) *Antisense Nucleic Acid Drug Dev. 10*, 53−61.
25. Mathews, D. H., Sabina, J., Zuker, M., and Turner, D. H. (1999) *J. Mol. Biol. 288*, 911−940.
26. Sakamoto, T., Tanaka, Y., Kuwabara, T., Kim, M. H., Kurihara, Y., Katahira, M., and Uesugi, S. (1997) *J. Biochem. 121*, 1123−1128.
27. Suh, Y. A., Kumar, P. K., Taira, K., and Nishikawa, S. (1993) *Nucleic Acids Res. 21*, 3277−3280.
28. Thill, G., Vasseur, M., and Tanner, N. K. (1993) *Biochemistry 32*, 4254−4262.
29. Duhamel, J., Liu, D. M., Evilia, C., Fleysh, N., Dinter-Gottlieb, G., and Lu, P. (1996) *Nucleic Acids Res. 24*, 3911−3917.
30. Fersht, A. (1999) *Structure and Mechanism in Protein Science*, Freeman, New York.
31. Kuo, M. Y., Sharmeen, L., Dinter-Gottlieb, G., and Taylor, J. (1988) *J. Virol. 62*, 4439−4444.
32. Perrotta, A. T., and Been, M. D. (1990) *Nucleic Acids Res. 18*, 6821−6827.
33. Werner, M., and Uhlenbeck, O. C. (1995) *Nucleic Acids Res. 23*, 2092−2096.
34. Luptak, A., Ferre-D'Amare, A. R., Zhou, K., Zilm, K. W., and Doudna, J. A. (2001) *J. Am. Chem. Soc. 123*, 8447−8452.
35. Peracchi, A. (1999) *Nucleic Acids Res. 27*, 2875−2882.

BI011963T